Expectation of Ground Motion in Earthquake Early Warning using real time Monitoring of Wavefield – A Method without Hypocenter and Magnitude –

M. Hoshiba
Meteorological Research Institute, Japan

SUMMARY:
In many methods of present EEW systems, hypocenter and magnitude are determined quickly, after which ground motions are predicted. Although these methods can predict the strength of ground motions by using a few parameters (e.g., hypocenter, magnitude, and site factors), it is not easy to take the effects of rupture directivity and source extent into account. After the 2011 Tohoku earthquake (M_w9.0), multiple events occurred simultaneously, which made it difficult to accurately determine the hypocenters and magnitudes, and led to some false alarms. To address these problems, a new method is proposed that applies the Kirchhoff-Fresnel boundary integral equation. Ground motion is predicted from real-time ground motion observation at front stations in direction of incoming seismic waves. It is possible to predict ground motion without a hypocenter and magnitude. The effects of rupture directivity, source extent and simultaneous multiple events are substantially included in this method.

Keywords: Real time, Prediction of ground motion, Earthquake Early Warning, Boundary integral

1. INTRODCTION

The aim of Earthquake Early Warning, EEW, is to mitigate earthquake disasters by giving people enough time to take appropriate safety measures in advance of strong ground motion. EEW systems have been researched and developed in Japan, Mexico, the United States, Taiwan, Italy, Turkey, and other countries [e.g., Nakamura(1988), Hoshiba et al.(2008), Kamigaichi et al.(2009), Nakamura et al.(2009), Allen et al.(2009), Espinosa Aranda et al.(2009), Hsiao et al.(2009), Zollo et al.(2009), Alcik et al. (2009)].

The nationwide EEW system of Japan, which has been operated by the Japan Meteorological Agency (JMA) since 2007, adopts a network method using the seismic signals from more than 1,100 stations [Hoshiba et al.(2008)], in which hypocenter and magnitude, M, are rapidly determined at first and then ground motion is predicted using the hypocenter and M. Performance of the JMA EEW system for the 2011 off the Pacific coast Tohoku earthquake (the Tohoku earthquake, M_w9.0; March 11, 2011) has been reported by Hoshiba et al.(2011), and Hoshiba and Ozaki(2012). Everywhere in the Tohoku district, the JMA EEW was earlier than the S-wave arrival and more than 15 s earlier than the strong ground motion. That is, the system performed as designed for the Tohoku district. However, for the Kanto district around Tokyo (approximately 400km from the epicenter), the predicted intensity was smaller than the observed intensity. This under-prediction can be attributed to the large extent of the later fault rupture [Aoi et al.(2011a), Kurahashi and Irikura(2011)]. For several weeks after the mainshock, aftershocks sometimes occurred simultaneously over the wide source region. When this happened, the system became confused and did not always determine the location and M correctly, which led to some false alarms. The experience of the M_w9.0 Tohoku earthquake revealed weak points of the network method based on rapid estimation of hypocenter and M: large errors in hypocentral location and M led directly to large errors in predicted ground motion, and the system cannot proceed to a prediction of ground motion without hypocenter and M information.

In Japan, JMA operates approximately 200 strong-motion seismometers, and the National Research Institute for Earth Science and Disaster Prevention (NIED) deploys 1,800 instruments in K-NET and KiK-net [Okada et al.(2004)]. In the Kanto district around Tokyo, KiK-net sensors at 30 sites are installed at depths of 500-3,500m in boreholes, as well as at the ground surface. In addition, JMA and municipalities deploy seismic intensity meters, whose sensors are accelerometer, at approximately 400 and 2,800 sites, respectively. Some other organizations and private companies perform their own observations. While each network is composed of many stations, integrating them would create an even denser strong ground motion observation network.

In this presentation, I propose a new method of ground motion prediction for EEW that extends the front detection method based on the Kirchhoff boundary integral technique (or the Kirchhoff-Fresnel integral technique for high frequency approximation). This method can predict ground motion in real time without requiring hypocenter and *M* data, using a dense seismometer network.

2. METHOD

A dense seismometer network that transmits ground motion data in real time makes it possible to monitor seismic wave propagation in real time. Fig.2.1 shows an example of the monitoring for the case of the M_w9.0 Tohoku earthquake. Comparing snapshots several seconds apart gives an intuitive sense of the spreading of the waves, and wave propagation in the near future is easily visualized even without knowing the location of the hypocenter and *M*. Unlike network methods of EEW based on rapid estimation of hypocenter and *M*, in which the causes (hypocenter and *M*) are first identified and the prediction is then performed based on the identified causes, the proposed method is based on real-time monitoring of wave propagation (Fig. 2.1), and the prediction of ground motion skips the steps of estimating the hypocenter and *M*. Kuruk and Motosaka(2008) and Nagashima *et al.*(2008) have also discussed precise prediction of ground motion based on the forward use of front stations. Hoshiba *et al.*(2010) concluded that prediction using observations from neighboring front stations is more precise than that based on the hypocenter and *M*.

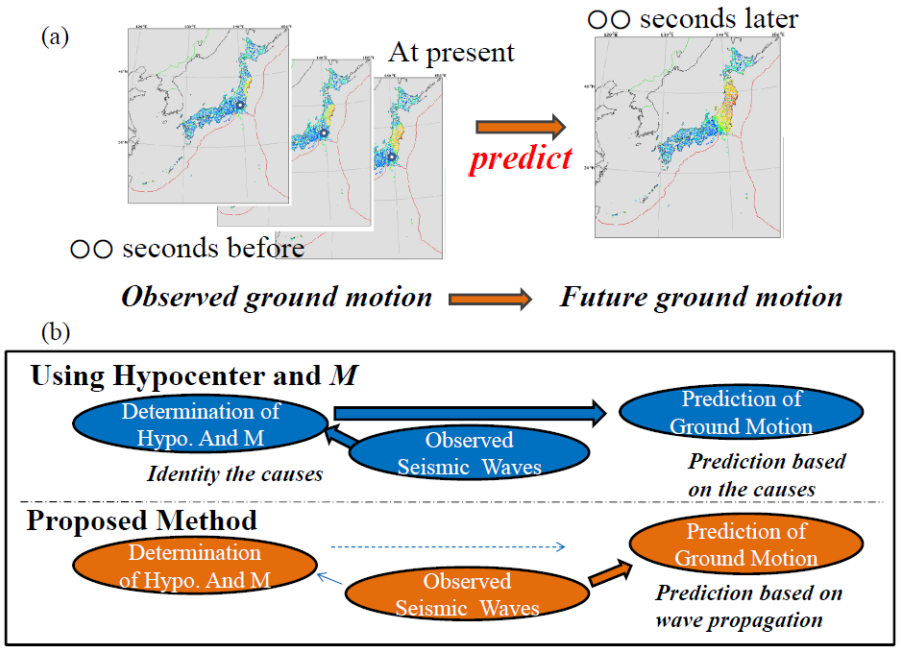

Figure 2.1. (a) Example of real-time monitoring of ground motion for the case of the M_w9.0 Tohoku earthquake. Red cross indicates the location of the hypocenter. (b) Comparison of the method proposed in this presentation with that using hypocenter and *M*.

2.1. Application of Huygens principle and Kirchhoff-Fresnel boundary Integral

Humans can envision the wave propagation for the near future when looking at a map view of real time monitoring. This intuitive form of prediction is probably based on extrapolation of the apparent velocity of wave propagation, and also Huygens' principle. Huygens' principle is a qualitative description of the physics of wave propagation, and Kirchhoff's boundary integral is the quantitative one, which is generally expressed as

$$u(\boldsymbol{r},t)=\int (u(\boldsymbol{r}_1,\tau)*\frac{\partial G(\boldsymbol{r},t,\boldsymbol{r}_1,\tau)}{\partial n}-G(\boldsymbol{r},t,\boldsymbol{r}_1,\tau)*\frac{\partial u(\boldsymbol{r}_1,\tau)}{\partial n})\,dS \qquad (1)$$

for scalar waves, in which $u(\boldsymbol{r}, t)$ is the wavefield at location $\boldsymbol{r}$ and time t, $\boldsymbol{r}$ is the location of the target point of the prediction, S is the surface enclosing $\boldsymbol{r}$, $\boldsymbol{r}_1$ is a location on S, $\partial/\partial n$ is the derivative with respect to the normal vector to S at $\boldsymbol{r}_1$, and G is the Green function. Here the integration is performed with respect to $\boldsymbol{r}_1$ on S, and * indicates the convolution integral with respect to τ. Equation (1) is valid when there are no radiations (that is, no sources) inside of surface S. When the wave length is much smaller than the spatial fluctuation of absolute amplitude of $u(\boldsymbol{r}, t)$ and $G(\boldsymbol{r}, t, \boldsymbol{r}_1, \tau)$, that is, in high frequency cases, equation (1) is approximated as Kirchhoff-Fresnel Integral,

$$u(\boldsymbol{r},t)\approx\int\frac{1}{v(\boldsymbol{r}_1)}(\cos\theta+\cos\theta')\;G(\boldsymbol{r},t,\boldsymbol{r}_1,\tau)\;*\dot{u}(\boldsymbol{r}_1,\tau)\,dS \qquad (2)$$

where $\theta(=\theta(\boldsymbol{r}_1, \tau))$ and $\theta'(=\theta'(\boldsymbol{r}_1))$ are the angle of incoming and outgoing ray paths from the surface normal, respectively, as shown in Fig. 2.2, and $v(\boldsymbol{r}_1)$ is the velocity at $\boldsymbol{r}_1$. Here θ' is determined by the geometries of S and $\boldsymbol{r}$, irrespective of the wavefield, so that θ' is a given parameter. The image of equation (2) is that the contributions from the secondary sources located on S produce the waveform at $\boldsymbol{r}$, which is qualitatively similar to Huygens' principle. Equations (1) and (2) make it possible to predict the waveforms at $\boldsymbol{r}$ and t when the time derivative of $u(\boldsymbol{r}_1, \tau)$ on S and their propagation directions, θ, are known on the condition that the Green function, G, and velocity, v, can be evaluated beforehand.

When velocity v is approximated as homogeneous, that is, $v(\boldsymbol{r})\approx v_0$, the Green function is expressed as

$$G(\boldsymbol{r},t,\boldsymbol{r}_1,\tau)\approx\frac{1}{4\pi|\boldsymbol{r}-\boldsymbol{r}_1|}\;\delta(t-\tau-\frac{|\boldsymbol{r}-\boldsymbol{r}_1|}{v_0}) \quad , \qquad (3)$$

and then equation (2) is approximated as

$$u(\boldsymbol{r},t)\approx\int\frac{1}{4\pi v_0|\boldsymbol{r}-\boldsymbol{r}_1|}(\cos\theta+\cos\theta')\;\dot{u}(\boldsymbol{r}_1,t-\frac{|\boldsymbol{r}-\boldsymbol{r}_1|}{v_0})\,dS \quad , \qquad (4)$$

where $\theta=\theta(\boldsymbol{r}_1, t-|\boldsymbol{r}-\boldsymbol{r}_1|/v_0)$. The waveform at time t is the summation of waveforms at time, $t-|\boldsymbol{r}-\boldsymbol{r}_1|/v_0$, so that the lead time for the prediction is $|\boldsymbol{r}-\boldsymbol{r}_1|/v_0$. Equation (4) means that the wavefield near the target point, $\boldsymbol{r}$, is used for the prediction of the near future (that is, small $|\boldsymbol{r}-\boldsymbol{r}_1|/v_0$), and the wavefield far from $\boldsymbol{r}$ is used for the distant future. Therefore small S and large S are used for predictions of the near and distant future, respectively.

In this presentation, I attempt to predict wave motions based on (1), (2) or (4). Because the prediction uses real time observation of waves approaching the target point, this method corresponds to a quantitative extension of the conventional front detection technique of EEW. Equation (1) and its approximations (2) and (4) are valid even for cases in which multiple sources exist (that is, multiple simultaneous earthquakes), or in which the waves are radiated from large areas (that is, large source extent), or in which the radiation is not isotropic (that is, strong directivity), when locations of all sources are outside of S. Therefore, this method is applicable to these cases.

2.2. Application for Small Lead Time

When the distance from the observing station to target point, $|\boldsymbol{r}-\boldsymbol{r}_1|$, is much smaller than the distance from the sources, that is, when S is small and the lead time is small, equations (1), (2) and (4) can be

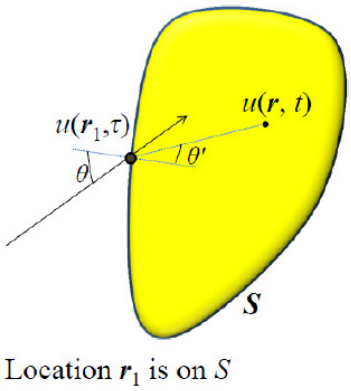

Figure 2.2. Definition of angles θ *and* θ' at $\boldsymbol{r}_1$ with respect to the target point $\boldsymbol{r}$ and the surface S.

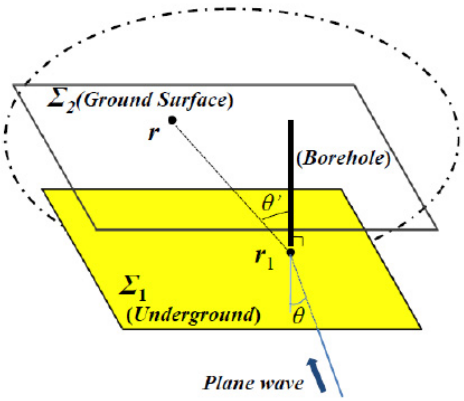

Figure 2.3. Two infinite planes (Σ_1 and Σ_2) are located in parallel, and the observed station ($\boldsymbol{r}_1$) and the target point ($\boldsymbol{r}$) are on Σ_1 and Σ_2, respectively. Surface S is composed of Σ_1 and an upper hemisphere of infinite radius.

expressed as a simpler approximation. Let us consider two parallel infinite planes (Σ_1 and Σ_2) as shown in Fig. 2.3, in which the observing station ($\boldsymbol{r}_1$) and the target point ($\boldsymbol{r}$) are located on Σ_1 and Σ_2, respectively. Surface S is composed by Σ_1 and an upper hemisphere of infinite radius. Contributions from the hemisphere are negligible, so those from Σ_1 are evaluated. Because the distance to the sources is much larger than $|\boldsymbol{r}\text{-}\boldsymbol{r}_1|$, plane wave incidence can be assumed around $\boldsymbol{r}_1$, equation (4) is given by

$$u(\boldsymbol{r},t) \approx u(\boldsymbol{r}_1, t - \frac{|\boldsymbol{r}-\boldsymbol{r}_1|}{v_0}\cos(\theta'-\theta)) \quad , \tag{5}$$

where (3) is used for the Green function. This means that the waveforms at $\boldsymbol{r}$ and those at $\boldsymbol{r}_1$ are the same after correction for travel time. This relation is easily inferred because of the plane wave propagation. For real applications in seismology and earthquake engineering, however, site amplification factors should be taken into account,

$$u(\boldsymbol{r},t) \approx f(t) * u(\boldsymbol{r}_1, t - \frac{|\boldsymbol{r}-\boldsymbol{r}_1|}{v_0}\cos(\theta'-\theta)) \tag{6}$$

where $f(t)$ is the time series representing the site amplification factors.

An example of such a case is the prediction of waveforms at the ground surface using borehole observations. In Fig. 2.3, Σ_1 and Σ_2 correspond to an infinite horizontal plane at the depth of the borehole sensor and the ground surface, respectively. As described in Section 1, 30 stations of KiK-net of NIED have borehole accelerometers at depths of 500-3,500m in the Kanto district.

3. EXMAPLE OF THE APPLICATION

As described in Section 1, quite dense seismic networks of strong ground motion stations can be realized by combining the existing networks of some organizations. At present, some stations transmit the data continuously in real time, but others record the waveform data using triggers. While trigger-type stations do not send out waveforms data in real time, some do continuously transmit representative parameters of waveforms such as seismic intensity [Aoi et al.(2008)], because their data volume is much smaller than that of the full waveform. In Japan, the JMA scale is usually used for seismic intensity, which is obtained from three-component accelerograms. JMA intensity is defined as the logarithm of vector amplitude after filtering of around 0.5Hz; details have been explained by Hoshiba and Ozaki(2012) and Hoshiba et al.(2010). For example application of the extended front detection method, in this section I use these seismic intensity data instead of waveform data, taking the current situation of available data into account. When we focus on a certain frequency band around ω_c

of seismic waves, $f(t)$ does not have a long tail along t for high frequencies. Seismic intensity on the JMA scale is basically evaluated from the logarithm of waveform amplitude; thus (6) may be described as an intensity expression,

$$I(\boldsymbol{r},t) \approx F_0 + I(\boldsymbol{r}_1, t - \frac{|\boldsymbol{r}-\boldsymbol{r}_1|}{v_0}\cos(\theta'-\theta)) \quad (7)$$

where $I(\boldsymbol{r}, t)$ is the seismic intensity, and F_0 corresponds to the logarithm of the site amplification factor around ω_c.

3.1. Case of Small *S* in which θ can be Assumed (Borehole case)

As described in Section 2.2, a borehole is an example of small *S*, in which we may assume a vertical plane wave incidence ($\theta \approx 0$). Seismic intensity at the surface will be predicted using borehole observation. Fig.3.1(left) shows examples using station TKYH11 (KiK-net) from the *M*6.0 event (23 July, 2005; focal depth is 73km; epicentral distance of 30km), where seismic waves are observed in borehole (3000m) and surface. F_0 for this station was empirically evaluated to be 1.8 using past data [Iwakiri et al.(2012)]. Borehole sensors are installed directly below the surface sensors, so that $\theta'=0$, and S wave arrival times differ by approximately 3.0s between the borehole and surface sensors [Iwakiri et al.,(2012)], that is $|\boldsymbol{r}-\boldsymbol{r}_1|/v_0 \approx 3.0$s. Fig.3.1(a) indicates the seismic intensity at the surface and in the borehole, the latter before and after applying the site amplification factor of 1.8. The borehole data yield a precise prediction of ground motion at the surface with a short lead time, approximately 3.0s.

3.2. Case of small *S* in which θ cannot be assumed

Subsection 3.1 is the case where θ is known, or can be assumed. In this subsection, we will describe again the case of small *S*, but for unknown θ. Here $|\boldsymbol{r}-\boldsymbol{r}_1|$ is assumed again to be small compared to the distance from the source, so that plane wave incidence is assumed. With small aperture arrays, it is possible to estimate propagation direction θ, but many arrays are not realistic at present. In this case, EEW should be based on the most severe scenarios as found by assuming various values of θ. For example,

$$I(\boldsymbol{r},t) \approx \max_i \{F_{0i} + I(\boldsymbol{r}_i, t - \frac{|\boldsymbol{r}-\boldsymbol{r}_i|}{v_0})\} \quad (8)$$

is a candidate, where $\boldsymbol{r}_i$ is the location of the *i*-th observing station and F_{0i} is the site amplification factor at the *i*-th station in terms of seismic intensity. This is similar to the idea proposed by Aoi et al.(2011b) and Kanjo(2011). Fig. 3.1(b) shows an example using the waveform data of the M_w9.0 Tohoku earthquake, in which station TKY013 (K-net) is the target point of the prediction. The neighbour stations up to $|\boldsymbol{r}-\boldsymbol{r}_i| \approx 35$km are used, so that the lead time is up to approximately 10 s, and $F_{0i}=0$ is assumed in the figure. The prediction (red line), based on (8), predicts the observations (blue line) about 10 s in advance although intensities are slightly over-predicted because it is the maximum value among the neighbour stations, especially after the peak of ground motion.

The special case of $|\boldsymbol{r}-\boldsymbol{r}_i| \to 0$ corresponds to the prediction based on waveforms observed at the target point itself, in which EEW will be issued just after its criterion is satisfied. In this case, the lead time is 0, but it indicates that we can avoid a complete “missed alarm” which means that EEW is not issued despite the actual occurrence of strong ground motion.

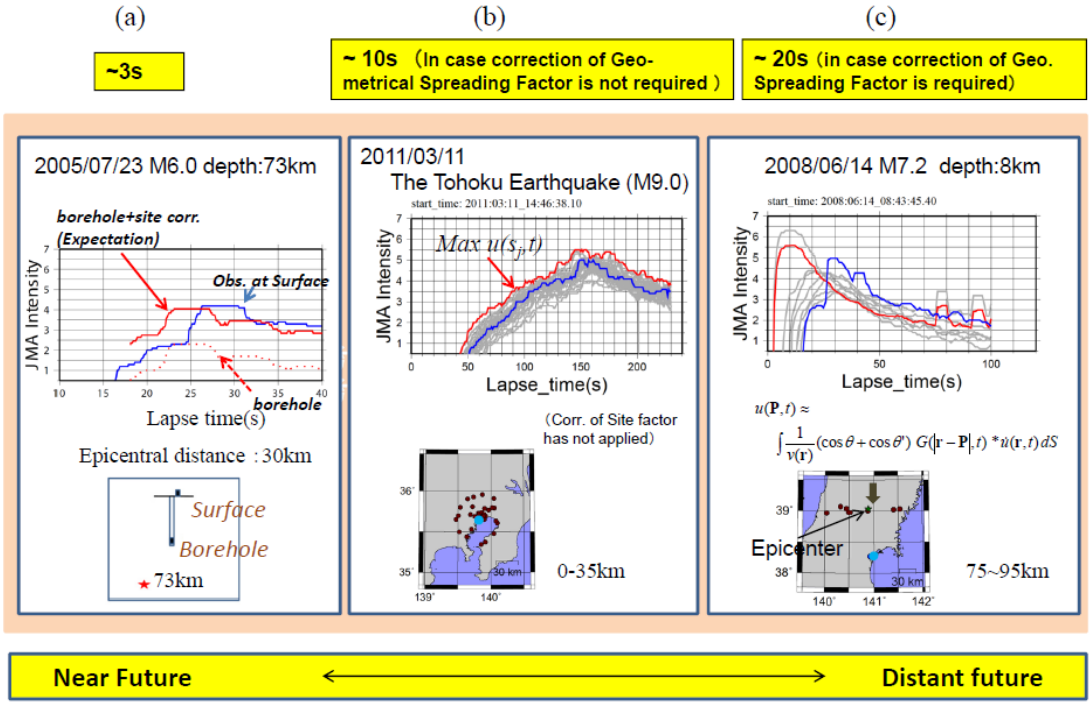

Figure 3.1. Examples of real time prediction of ground motion. (a) using borehole (3000m) data. Dotted red and solid blue lines indicate the seismic intensity (on JMA scale) at borehole and at surface, respectively. Solid red line represents the seismic intensity observed at borehole after the correction of site amplification factor. Here the seismic intensity is estimated from Kunugi et al's(2008) technique. (b) prediction of seismic intensity using equation (8). Red and blue lines indicate the predicted and observed seismic intensity, respectively. Gray lines indicate the seismic intensity of the neighbor stations. (c) prediction using equation (4).

3.3. Case of large *S*

When a long lead time is desired, a large S is used. In this case, $|\boldsymbol{r}-\boldsymbol{r}_1|$ is not assumed to be small relative to the hypocentral distance, and plane wave incidence cannot be assumed. At first in this subsection, we assume that wave propagation direction θ is known or can be assumed. In this case, equation (2) or (4) is used for real-time prediction of ground motion, and we need to introduce some assumptions for performing the integration, considering the current situation of data availability as described above. Though the wavefield at the ground surface is observable when dense stations of strong ground motion are deployed at the surface, the wavefield underground cannot be observed at depths below a few kilometers. Some assumptions are required for the underground wavefield. For simplicity we assume ground motion that does not vary with depth, that is, $u(\boldsymbol{r}, t)=u(x, y, z, t)=u(x, y, 0, t)$, in this presentation for the application of (4). Here z represents the depth.

Fig. 3.1(c) shows examples of M 7.2 Iwate Miyagi Nairiku earthquake (14 June, 2008; focal depth 8km). The target point is MYG013 (K-NET), and an incident angle from due north is assumed. This figure shows the prediction based on equation (4) using stations 75-95km from MYG013, corresponding to lead time of approximately 20s. I assumed in the above discussion that θ is known (or that data exist to specifyθ). If θ is unknown, the maximum strength of the predicted ground motion is found by assuming various values of θ. When we have many arrays which give us the information of θ, (2) and (4) could be applicable with the observed θ.

3.4. Continuous Prediction

From the observed wavefield at $t=t_c-\Delta t$, using equations (1), (2) or (4) it is possible to estimate the future wavefield at $t=t_c$ at even places where seismometers are not installed. The predicted wavefield at $t=t_c$ will be used for the estimation of the wavefield at $t=t_c+\Delta t$ combined with real observation by seismometers. This process is a kind of data assimilation which is widely used in the weather forecast technique. Fig. 3.2 schematically shows the data stream and the process of the prediction. Even when

no ground motion is observed, it is an observation; and when no shaking is predicted, it is a prediction. Continuous prediction using the data assimilation technique will improve the preciseness of the prediction of ground motion.

4. CONCLUSION

I have proposed a method for real-time prediction of ground motion using real-time monitoring of ground motion, extending the front detection method for application to EEW. The basic idea is from Huygens' principle as quantified using Kirchhoff-Fresnel boundary integral. Although this method requires a dense observation network, it becomes possible to predict ground motion without waiting for a hypocenter and magnitude to be determined, because these source parameters are not necessary. The effects of rupture directivity, source extent and simultaneous multiple events can also be substantially included in this method.

The proposed method enables predictions to include more information about the timing of ground motion. When predictions 3s in advance are required, borehole observations are useful for precise predictions, as described in subsection 3.1, which is applicable in the Kanto district around Tokyo where 30 existing borehole stations are at depths of 500-3500 m. When a longer lead time (~10s) is required, neighbor stations around the target point can be used at distances less than approximately 35 km, as explained in subsection 3.2. For longer lead times, information from more distant stations can be used, as discussed in subsection 3.3.

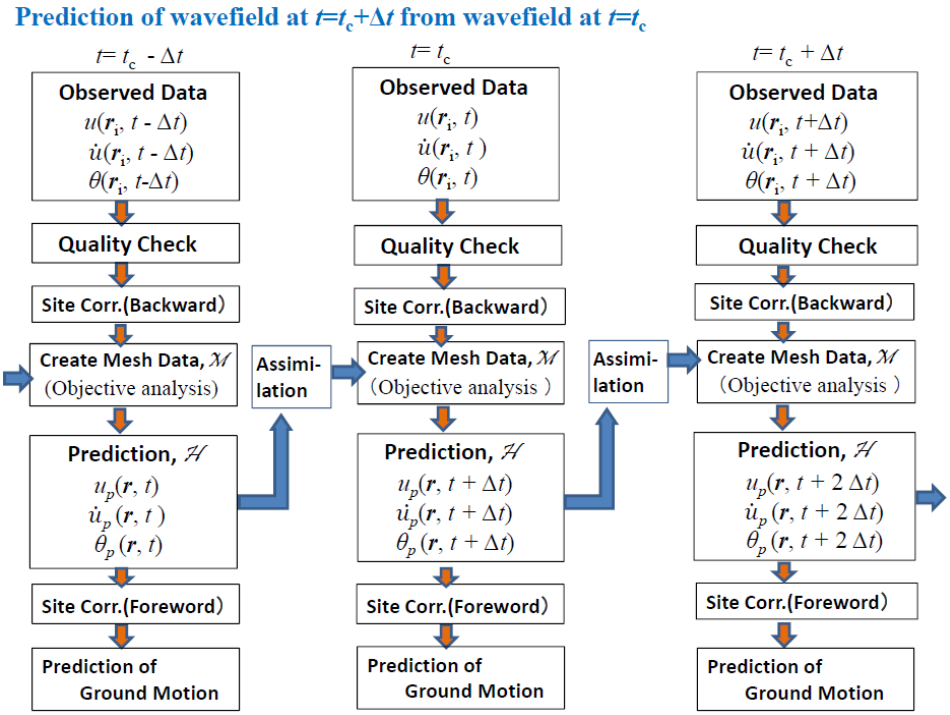

Figure 3.2. Schematically shown continuous prediction of ground motion using objective analysis, data assimilation, and real time site correction.

AKCNOWLEDGEMENT
I thank A. Katsumata, K. Iwakiri and N. Hayashimoto for their help in completing the figures. Seismic intensity data were provided by JMA, NIED and local governments and municipalities. Waveform data were obtained from the JMA network, K-NET and KiK-net of NIED. The unified hypocenter catalog and CMT catalog of JMA were used in this analysis. Figures were made using Generic Mapping Tools [Wessel and Smith(1995)].

REFERENCES

Alcik, H., Ozel, O., Apaydin, N. and Erdik, M. (2009). A study on warning algorithms for Istanbul earthquake early warning system, *Geophys. Res. Lett.*, **36**, L00B05, doi:10.1029/2008GL036659.

Allen, R., Brown, H., Hellweg, M., Khainovski, O., Lombard P. and Newhauser, D. (2009a). Real-time earthquake detection and hazard assessment by ElarmS across California, *Geophysical Research. Letters*, **36**, L00B08, doi:10.1029/2008GL036766.

Aoi S., Kunugi, T., Adachi, S., Nakamura, H., Morikawa, N., Obara, K. and Fujiwara, H. (2008). Deployment of new strong-motion seismographs of KiK-net, 2008 meeting of Japan Geoscience Union, S146-004.

Aoi S., Kunugi, T., Suzuki, W., Morikawa, M., Nakamura, H. and Fujiwara, H. (2011a). Strong ground motions from the 2011 off the Pacific coast of Tohoku Earthquake (in Japanese), *Bulletin of JAEE*, **15**, 25-28.

Aoi S., Kunugi, T., Nakamura, H., Suzuki, W. and Fujiwara, H. (2011b). Real time monitoring of strong ground motion, ERI Meeting of "Rapid analysis and prediction of seismic ground motion", http://wwweic.eri.u-tokyo.ac.jp/ viewdoc (in Japanese, last accessed Jan. 11, 2012).

Espinosa Aranda, J.M., Cuellar, A., Ibarrola, G., Garcia, A., Maldonado, S. and Rodriguez, F.H. (2009). Evolution of the Mexican seismic alert system (SASMEX), *Seismological Research Letters*, **80**, 694-706.

Hoshiba, M., Kamigaichi, O., Saito, O., Tsukada, S. and Hamada, N. (2008). Earthquake early warning starts nationwide in Japan, *EOS Trans*, *AGU*, **89**, 73-74.

Hoshiba, M., Ohtake, K., Iwakiri, K., Aketagawa, T., Nakamura, H. and Yamamoto, S.(2010). How precisely can we anticipate seismic intensities? A study of uncertainty of anticipated seismic intensities for the Earthquake Early Warning method in Japan, *Earth Planets Space*, **62**, 611-620.

Hoshiba, M., Iwakiri, K., Hayashimoto, N., Shimoyama, T., Hirano, K., Yamada, Y., Ishigaki, Y. and Kikuta H. (2011). Outline of the 2011 off the Pacific coast of Tohoku Earthquake (M_w 9.0) —Earthquake Early Warning and observed seismic intensity—, *Earth Plants Spaces*, **63**, 547-551.

Hoshiba, M. and Ozaki, T. (2012). Earthquake Early Warning and Tsunami warning of JMA of the 2011 off the Pacific coast of Tohoku Earthquake (in Japanese), *Zisin 2*. **64**, 155-168.

Hsiao, N.C., Wu, Y.M., Shin, T.C., Zhao, L. and Teng, T.L. (2009). Development of earthquake early warning system in Taiwan, *Geophys. Res. Lett.*, **36**, L00B02, doi:10.1029/2008GL036596.

Iwakiri, K., Hoshiba, M., Ohtake, K. and Shimoyama, T. (2012). Application of strong motion data observed in and around southern Kanto to the earthquake early warning (in Japanese), *Kenshinjiho* (*Japan Meteorological Agency*), **75**, 37-59.

Kamigaichi, O., Saito, M., Doi, K., Matsumori, T., Tsukada, S., Takeda, K., Shimoyama, T., Nakamura, K., Kiyomoto, M. and Watanabe,Y. (2009). Earthquake Early Warning in Japan – Warning the general public and future prospects -, *Seismological Research Letters*, **80**, 717-726.

Kanjo, K. (2011). Improvement of the accuracy and speed of the Earthquake Early Warning which adapted the real-time data. ERI Meeting of "Rapid analysis and prediction of seismic ground motion", http://wwweic.eri.u-tokyo.ac.jp/viewdoc/ yure2011/14_kanjyo.pdf (in Japanese, last accessed Feb. 7, 2012).

Kurahashi, S. and Irikura, K. (2011). Source model for generating strong ground motions during the 2011 off the Pacific coast of Tohoku Earthquake, *Earth Plants Spaces*, **63**, 571-576.

Kunugi, T., Aoi, S., Nakamura, H., Fujiwara H., and Morikawa, N. (2008), A real-time processing of seismic intensity (in Japanese), *Zisin 2*, **60**, 243-252.

Kuruk, H.S., and Motosaka. M. (2009). Real-time ground motion forecasting using front-site waveform data based on artificial neural network, *Journal of Disaster Research*, **4**, 260-266.

Nakamura, Y. (1988), On the urgent earthquake detection and alarm system (UrEDAS), *Proceedings of ninth world conference on earthquake engineering*, **7**, 673-678.

Nagashima, I., Yoshimura, C., Uchiyama, Y., Maseki R., and Itoi, T.(2008). Real-time prediction of earthquake ground motion using empirical transfer function, *Proceedings of 14th world conference on earthquake engineering*, S02-023.

Okada,Y., Kasahara, K., Hori, S., Obara, K., Sekiguchi, S., Fujiwara, H. and Yamamoto, A. (2004). Recent progress of seismic observation networks in Japan –Hi-net, F-net, K-NET and KiK-net, *Earth Planets Space*, **56**, xv-xxviii.

Wessel, P. and Smith, W.H.F. (1995), New version of the generic mapping tool released. *EOS Trans., AGU*, **76**, 329.

Zollo, A., Iannaccone, G., Lancieri, M., Cantore, L., Convertito, V., Emolo, A., Festa, G., Gallovič, F., Vassallo, M., Martino, C., Satriano, C. and Gasparini, P. (2009). Earthquake early warning system in southern Italy: Methodologies and performance evaluation, *Geophysical Research Letters*, **36**, L00B07, doi:10.1029/2008GL036689.